constraining to produce collective behavior. Indeed, we have found that at small values of s, the order parameter distribution for the KA mixture ceases to be bimodal when k_BT/ε is significantly larger than 1 (*18*). One possibility is that the first-order coexistence line ends at an upper critical point at finite s and T. This possibility remains to be investigated.

The first-order transition we have described is to be contrasted with the scenario that emerges from other approaches, such as mode-coupling theory (*26*, *27*) and the random first-order transition theory (*28*, *29*). These theories predict the existence of dynamic or thermodynamic transitions controlled by thermodynamic fields such as temperature or pressure. In contrast, our results show that the order-disorder transition is in the trajectories of the dynamics and is thus controlled by dynamic fields. Perhaps a thermodynamic manifestation can be related to the picture of an avoided phase transition (*30*). In any case, our numerical results here suggest that in real glass formers this dynamical order-disorder phenomenon is close to that predicted from idealized kinetically constrained models (*7*–*9*). Thus, we pass the baton to the experimenters to find protocols for controlling the dynamic observable K or driving field s that allow experimental probes of the transition described in this work.

References and Notes

1. M. D. Ediger, C. A. Angell, S. Nagel, *J. Phys. Chem.* **100**, 13200 (1996).
2. P. G. Debenedetti, F. H. Stillinger, *Nature* **410**, 259 (2001).
3. K. Schmidt-Rohr, H. Spiess, *Phys. Rev. Lett.* **66**, 3020 (1991).
4. E. R. Weeks, J. C. Crocker, A. C. Levitt, A. Schofield, D. A. Weitz, *Science* **287**, 627 (2000).
5. M. D. Ediger, *Annu. Rev. Phys. Chem.* **51**, 99 (2000).
6. S. C. Glotzer, *J. Non-Cryst. Solids* **274**, 342 (2000).
7. M. Merolle, J. P. Garrahan, D. Chandler, *Proc. Natl. Acad. Sci. U.S.A.* **102**, 10837 (2005).
8. R. L. Jack, J. P. Garrahan, D. Chandler, *J. Chem. Phys.* **125**, 184509 (2006).
9. J. P. Garrahan *et al.*, *Phys. Rev. Lett.* **98**, 195702 (2007).
10. P. G. Bolhuis, D. Chandler, C. Dellago, P. L. Geissler, *Annu. Rev. Phys. Chem.* **53**, 291 (2002).
11. D. Chandler, *Introduction to Modern Statistical Mechanics* (Oxford Univ. Press, Oxford, 1987).
12. D. P. Landau, K. Binder, *A Guide to Monte Carlo Simulations in Statistical Physics* (Cambridge Univ. Press, Cambridge, 2000); see section 4.2.3.
13. J.-P. Eckmann, D. Ruelle, *Rev. Mod. Phys.* **57**, 617 (1985).
14. V. Lecomte, C. Appert-Rolland, F. van Wijland, *J. Stat. Phys.* **127**, 51 (2007).
15. S. F. Swallen *et al.*, *Science* **315**, 353 (2007); published online 6 December 2006 (10.1126/science.1135795).
16. F. Ritort, P. Sollich, *Adv. Phys.* **52**, 219 (2003).
17. W. Kob, H. C. Andersen, *Phys. Rev. Lett.* **73**, 1376 (1994).
18. Supporting materials are available for this article on *Science* Online.
19. J. D. Honeycutt, H. C. Andersen, *J. Phys. Chem.* **91**, 4950 (1987).
20. C. Borgs, R. Kotecky, *Phys. Rev. Lett.* **68**, 1738 (1992).
21. J. P. Hansen, I. R. McDonald, *The Theory of Simple Liquids* (Academic Press, London, 2006).
22. S. F. Edwards, P. W. Anderson, *J. Phys. F* **5**, 965 (1975).
23. B. Doliwa, A. Heuer, *Phys. Rev. E* **67**, 031506 (2003).
24. G. A. Appignanesi, J. A. Rodríguez Fris, R. A. Montani, W. Kob, *Phys. Rev. Lett.* **96**, 057801 (2006).
25. H. Nakanishi, M. E. Fisher, *Phys. Rev. Lett.* **49**, 1565 (1982).
26. W. Gotze, L. Sjogren, *Rep. Prog. Phys.* **55**, 241 (1992).
27. D. R. Reichman, P. Charbonneau, *J. Stat. Mech.* **2005**, P05013 (2005).
28. T. R. Kirkpatrick, D. Thirumalai, P. Wolynes, *Phys. Rev. A* **40**, 1045 (1989).
29. J. P. Bouchaud, G. Biroli, *J. Chem. Phys.* **121**, 7347 (2004).
30. D. Kivelson, S. A. Kivelson, X. L. Zhao, Z. Nussinov, G. Tarjus, *Physica A* **219**, 27 (1995).

31. During the course of this work we have benefited from discussions with T. F. Miller III and F. van Wijland. The work was made possible through grants from the NSF (CHE-0543158 in the early stages for R.J. and D.C. and CHE-0626305 in the later stages for L.H. and D.C.), from the U.S. Office of Naval Research (N00014-07-1-0689 in the late stages for R.J.), and from the Engineering and Physical Sciences Research Council (GR/S54074/01 for J.P.G.).

Supporting Online Material

www.sciencemag.org/cgi/content/full/1166665/DC1
SOM Text
Figs. S1 to S4
References

1 October 2008; accepted 22 January 2009
Published online 5 February 2009;
10.1126/science.1166665
Include this information when citing this paper.

Functional Proteomics Identify Cornichon Proteins as Auxiliary Subunits of AMPA Receptors

Jochen Schwenk,[1]* Nadine Harmel,[1]* Gerd Zolles,[1]* Wolfgang Bildl,[1] Akos Kulik,[4] Bernd Heimrich,[4] Osamu Chisaka,[6] Peter Jonas,[3] Uwe Schulte,[1,2] Bernd Fakler,[1,5]† Nikolaj Klöcker[1]†

Glutamate receptors of the AMPA-subtype (AMPARs), together with the transmembrane AMPAR regulatory proteins (TARPs), mediate fast excitatory synaptic transmission in the mammalian brain. Here, we show by proteomic analysis that the majority of AMPARs in the rat brain are coassembled with two members of the cornichon family of transmembrane proteins, rather than with the TARPs. Coassembly with cornichon homologs 2 and 3 affects AMPARs in two ways: Cornichons increase surface expression of AMPARs, and they alter channel gating by markedly slowing deactivation and desensitization kinetics. These results demonstrate that cornichons are intrinsic auxiliary subunits of native AMPARs and provide previously unknown molecular determinants for glutamatergic neurotransmission in the central nervous system.

Fast excitatory synaptic transmission in the mammalian CNS is mostly mediated by AMPA receptors (AMPARs), ligand-gated ion channels that are activated by glutamate released from the presynaptic terminals (*1*–*4*). On activation, AMPARs provide the transient excitatory postsynaptic current (EPSC) that depolarizes the membrane and initiates downstream processes, such as the generation of action potentials or synaptic plasticity (*5*, *6*). The time course and amplitude of AMPAR-mediated EPSCs exhibit considerable variability among neurons and synapses and strongly depend on the properties of the postsynaptic AMPARs (*7*, *8*).

AMPARs are tetrameric assemblies of α subunits with distinct properties that are encoded by the glutamate receptor (GluR) genes GluR-A to GluR-D (*9*–*11*) [or GluA1-4 according to the International Union of Basic and Clinical Pharmacology nomenclature (*12*)] and their variations resulting from alternative splicing and RNA editing (*13*–*15*). In most central neurons, multiple variants of these GluR proteins are expressed and assembled into heteromultimeric channels that display a wide range of gating kinetics and Ca^{2+} permeabilities (*16*–*19*). In addition to the α subunits, the properties of the AMPARs are modulated by a family of transmembrane AMPAR regulatory proteins (TARPs) (*20*, *21*). The TARPs coassemble with the GluR proteins and through direct protein-protein interactions affect the gating, permeability and pharmacology of the AMPARs (*21*–*25*). Furthermore, the TARPs influence the number and subcellular localization of AMPARs by promoting their trafficking to the plasma membrane and their targeting to the synapse (*26*, *27*).

The profound impact of the TARPs led to the assumption that almost all AMPARs in the mammalian brain may be assembled with these auxiliary subunits (*28*, *29*). However, only a minor portion of the AMPAR complexes in the rat brain (~30%) are associated with γ-2 and γ-3, the TARPs with the most widespread expression pattern (*30*, *31*) (Fig. 1A, arrowhead). It is, therefore, possible that native AMPARs contain further yet-unknown protein constituents that may be iden-

[1]Institute of Physiology II, University of Freiburg, Engesserstrasse 4, 79108 Freiburg, Germany. [2]Logopharm GmbH, Engesserstrasse 4, 79108 Freiburg, Germany. [3]Institute of Physiology I, University of Freiburg, Engesserstrasse 4, 79108 Freiburg, Germany. [4]Institute of Anatomy and Cell Biology, University of Freiburg, Albertstrasse 23, 79104 Freiburg, Germany. [5]Center for Biological Signaling Studies (bioss), Albertstrasse 10, 79104 Freiburg, Germany. [6]Department of Cell and Developmental Biology, Kyoto University, Kyoto 606-8502, Japan.

*These authors contributed equally to this work.
†To whom correspondence should be addressed. E-mail: bernd.fakler@physiologie.uni-freiburg.de (B.F.) or nikolaj.kloecker@physiologie.uni-freiburg.de (N.K.)

tified in a proteomic approach combining affinity purification of protein complexes and mass spectrometric analysis of their subunit composition. Such comprehensive analysis has successfully been applied to multiprotein complexes associated with different types of ion channels (*32*–*35*) but has not yet been performed with AMPARs.

Proteomic analysis of AMPAR complexes from rat brain. For proteomic analysis of native AMPARs, we used affinity purifications (APs) with three different antibodies specific either for GluR-A and GluR-B (anti–GluR-A, anti–GluR-B) or the TARPs γ-2 and γ-3 (anti–γ-2/3) (fig. S2, B and C) on solubilized membrane fractions prepared from total rat brain (*36*) (fig. S3). These protein preparations contained high-molecular-weight complexes of AMPARs (~0.7 megadalton) assembled from GluR and TARP subunits as visualized by two-dimensional gel separations using blue native polyacrylamide gel electrophoresis (BN-PAGE) and denaturing SDS-PAGE (*36*) (Fig. 1A and fig. S1). Total eluates of APs with the AMPAR subunit–specific antibodies or several pools of preimmunization immunoglobulins G (IgGs) serving as negative controls were analyzed by high-resolution nanoflow liquid chromatography tandem mass spectrometry (nano-LC MS/MS). The results of these MS-analyses showed that all four GluR proteins (GluR-A to GluR-D) were specifically and abundantly [rPQ score and PQ_{norm} score, respectively] (*36*) retained by each of the three AMPAR subunit–specific antibodies (table S1); the peptides retrieved by mass spectrometry provided extensive coverage for the primary sequence of the individual GluR isoforms (61, 75, 56, and 52% for GluR-A to GluR-D, respectively). Moreover, MS/MS spectra obtained from both anti-GluR and anti–γ-2/3 eluates identified five members of the TARP family, with significant peptide yields for γ-2 and γ-3, and smaller yields for γ-4, γ-7, and γ-8 (table S1). A sixth TARP isoform, γ-5, was only observed in eluates of anti–GluR-A APs, albeit in small amounts (table S1).

In addition to the known AMPAR subunits, our MS analyses consistently identified cornichon homolog 2 (CNIH-2) (Fig. 1B) and cornichon homolog 3 (CNIH-3), closely related members of a conserved family of small transmembrane proteins that was first described in *Drosophila* (Fig. 1, C and D) (*37*–*39*). Both cornichon proteins were specifically copurified at high yield with all three AMPAR subunit–specific antibodies (table S1), which suggests that CNIH-2 and CNIH-3 are robustly integrated into AMPAR complexes in rat brain.

Coassembly of native and heterologously expressed AMPARs and cornichon proteins. Coassembly of the two cornichon proteins with native AMPARs was confirmed by subsequent reverse-purification using an antibody specific for CNIH-2 and CNIH-3 (anti–CNIH-2/3) (fig. S2A) (*36*) on membrane fractions from rat brain. The respective eluates, besides the cornichon homologs, contained the AMPAR α subunits GluR-A to GluR-D, as well as the TARP isoforms γ-2, γ-3, and γ-4 (table S1). In addition, the cornichon-AMPAR assembly was corroborated by Western probing of the two-dimensional gel separation of the antibody-shift assay from Fig. 1A with the anti–CNIH-2/3 antibody; this assay separated the γ-2/3–associated AMPARs from those devoid of these TARPs by the additional mass introduced via target-specific binding of the anti–γ-2/3 IgG before the BN-PAGE. The major portion of the two cornichon proteins was not shifted by the γ-2/3 antibody, which indicated that CNIH-2 and CNIH-3 are predominantly assembled into γ-2/3–free AMPAR complexes (Fig. 2A). These γ-2/3–free AMPAR complexes were effectively and completely shifted when anti–CNIH-2/3 IgG was used

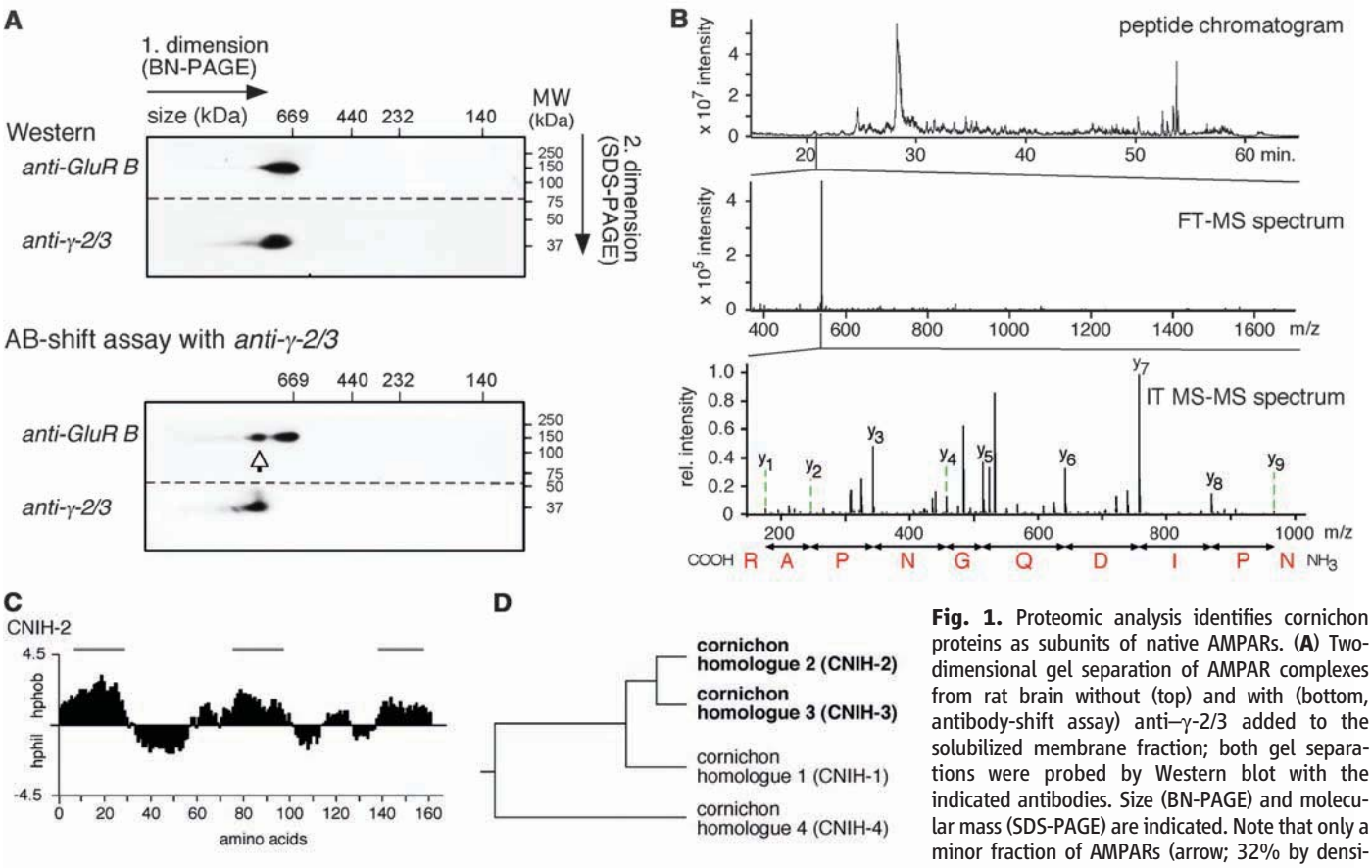

Fig. 1. Proteomic analysis identifies cornichon proteins as subunits of native AMPARs. (**A**) Two-dimensional gel separation of AMPAR complexes from rat brain without (top) and with (bottom, antibody-shift assay) anti–γ-2/3 added to the solubilized membrane fraction; both gel separations were probed by Western blot with the indicated antibodies. Size (BN-PAGE) and molecular mass (SDS-PAGE) are indicated. Note that only a minor fraction of AMPARs (arrow; 32% by densitometric analysis) is shifted by the anti–γ-2/3 antibody. (**B**) (Top) High-performance liquid chromatography chromatogram of peptide fragments of an anti–GluR-B eluate. (Middle and bottom) MS- and MS/MS-spectra of a peptide unique for CNIH-2 (*m/z* value of 541.27246). The complete MS/MS fragment y^+-ion series is indicated together with the amino acid sequence derived from the mass differences (in carboxy-to-amino-terminal direction). (**C**) Hydropathy plot (Kyte-Doolittle, window of 12 amino acids) of the rat CNIH-2 protein; horizontal bars denote sequence stretches long enough to span the membrane. (**D**) Dendrogram (Clustal method) of the cornichon family of proteins.

in the antibody-shift assay (fig. S4), which strongly suggested that all AMPARs not associated with TARPs are coassembled with CNIH proteins.

The participation of cornichons and TARPs in native AMPARs was further investigated by relative quantification of CNIH-2 and γ-2 protein in the aforementioned APs. The mass traces (*m/z* peak volumes) of peptides unique for CNIH-2 and γ-2 were quantified on the basis of calibration curves determined for these peptides in a dilution series with heterologously expressed tagged versions of both proteins (*36*). In APs with anti–GluR-A and anti–GluR-B, the ratio of copurified CNIH-2/γ-2 was between 6/1 and 7/1 (Fig. 2B) or, equivalently, ~85% of the purified AMPARs were associated with CNIH-2, whereas ~15% partnered with the TARP γ-2. The excess of copurified CNIH-2 over γ-2 was independent of the GluR composition of the AMPARs (Fig. 2B) and suggested that cornichons, similar to TARP proteins, may be directly assembled with the GluR subunits (*25*). This was tested in APs with anti–GluR-A and anti–CNIH-2/3 on membrane fractions prepared from *Xenopus* oocytes and cultured cells (*36*) that heterologously expressed CNIH-2 and heteromeric GluR-A/GluR-B AMPARs either alone or in combination. Robust and specific copurification of GluR-A and CNIH-2 was observed with both antibodies when used on oocytes coexpressing AMPARs and CNIH-2 (Fig. 2C).

Together, proteomic and biochemical analyses indicated that the cornichon proteins CNIH-2 and CNIH-3 are integral constituents of the majority of native AMPARs. They are intimately associated with the pore-forming GluR subunits.

Expression profile of cornichons in the CNS. Next, the expression profile of CNIH-2 and CNIH-3 in the rat brain was investigated by immunohistochemistry using the anti–CNIH-2/3 antibody. Anti–CNIH-2/3 immunoreactivity was observed throughout most regions of the brain. Examples of expression of CNIH-2/3 in the neocortex, hippocampal formation, and cerebellum are depicted in Fig. 3. In all these areas, CNIH-2/3 immunoreactivity was found in various types of neurons, including neocortical and hippocampal pyramidal cells and cerebellar Purkinje cells, as well as in glial cells, such as Bergmann glia in the cerebellum or astrocytes in the hippocampus (Fig. 3, A and B). Neither of the two cornichon proteins was detected in cerebellar granule cells [(Fig. 3A), right], where AMPAR-mediated synaptic transmission crucially depends on the presence of the TARP γ-2 (*40*, *41*). In the hippocampal CA1 region, the anti–CNIH-2/3 immunoreactivity was localized to the plasma membrane of both postsynapses and extrasynaptic sites (dendritic shafts, spines of pyramidal cells), as seen with post-embedding immunogold electron microscopy (EM) (Fig. 3C).

Enhanced surface expression of AMPARs by cornichons. Auxiliary subunits affect both processing and biophysical characteristics of the pore-forming α subunits of various ion channels (*42*), which prompts respective analyses for the cornichon proteins. To examine CNIH-mediated effects on AMPAR trafficking, we used heterologous expression of the flop splice variant of GluR-A (GluR-A_o) in cultured cells and *Xenopus* oocytes either alone or together with CNIH-2 or CNIH-3. Surface expression of the resulting AMPARs was monitored either by staining a hemagglutinin (HA) epitope in the extracellular N terminus of GluR-A_o (cultured cells) or by recording glutamate-activated currents in whole oocytes (*36*). Coexpression of either cornichon isoform markedly enhanced the HA-based surface immunoreactivity (Fig. 4A); quantification yielded an ~10-fold increase of GluR-A_o receptors in the plasma membrane of the CNIH-expressing cells (Fig. 4B). Similarly, in *Xenopus* oocytes coexpression of CNIH-2 or CNIH-3 substantially increased the GluR-A_o–mediated currents evoked by application of a saturating concentration of glutamate (1 mM) together with trichloromethiazide (TCM), an inhibitor of channel desensitization (*43*) (Fig. 4, C and D). In either system, the CNIH-mediated enhancement was highest at low expression levels of the homomeric AMPAR [(Fig. 4A), left] but decreased as the GluR-A_o expression was increased. Together, these results indicated that coassembly with CNIH-2 and CNIH-3 effectively promoted expression of the AMPAR complexes at the plasma membrane.

Modulation of AMPAR gating by cornichons. In addition to protein processing, whole-oocyte recordings showed that both cornichons markedly reduced the increase in current amplitude induced by TCM in the presence of glutamate (Fig. 4C). This reduction suggested that CNIH-2/3 may also influence the gating properties of the AMPARs.

The impact of the cornichon proteins on channel gating was investigated in giant outside-out (oo) patches from *Xenopus* oocytes with rapid glutamate application via a piezo-controlled fast application system (*36*, *44*). Figure 5A shows typical current transients recorded with 1-ms glutamate pulses on AMPARs assembled from GluR-A_i and GluR-B_i (GluR-A_i/B_i), a particularly abundant subunit combination in the CNS (*16*), either alone or in combination with the accessory subunits γ-2 or CNIH-2. All three types of AMPARs activated rapidly with similar values (means ± SD) for the 20 to 80% rise time (0.25 ± 0.03 ms, n = 11 for GluR-A_i/B_i; 0.32 ± 0.03 ms,

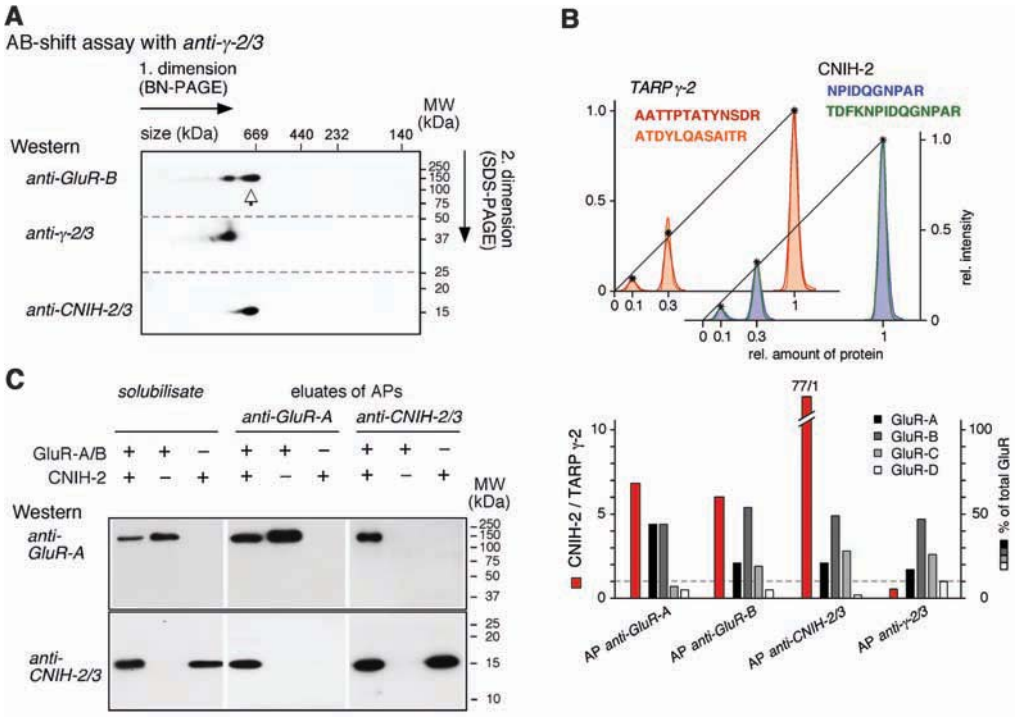

Fig. 2. Cornichons are major partners of AMPARs in the rat brain and directly coassemble with the AMPAR α subunits. (**A**) Antibody-shift assay from Fig. 1A probed by Western blot with the anti–CNIH-2/3 antibody. Note that the major portion of AMPARs (arrow) is associated with the cornichon proteins. (**B**) Relative quantification of AMPAR subunits in APs with the indicated antibodies. (Top) Calibration curves of *m/z* peak volumes used for relative quantification of CNIH-2 and γ-2 (*16*). Asterisks are intensity-weighted means of *m/z* peak volumes, lines represent linear regressions to these mean values. (Bottom) Molar ratio of CNIH-2 versus γ-2 (red bars) and GluR subunit composition in the indicated APs. (**C**) Copurification of AMPARs and CNIH-2 from *Xenopus* oocytes expressing GluR-A_i, GluR-B_i and CNIH-2. Solubilisate and eluates from APs with anti–GluR-A and anti–CNIH-2/3 were separated by SDS-PAGE and probed by Western blot with the indicated antibodies.

$n = 13$; 0.28 ± 0.04 ms, $n = 6$, for AMPARs with γ-2 and CNIH-2, respectively); however, they differed considerably in their deactivation kinetics, as reflected by the current decay when the agonist was removed (Fig. 5A, inset). Thus, either accessory subunit slowed the deactivation of GluR-A_i/B_i receptors, but, whereas slowing by γ-2 was moderate as reported earlier (*21*, *22*, *24*), deceleration by CNIH-2 was substantial and

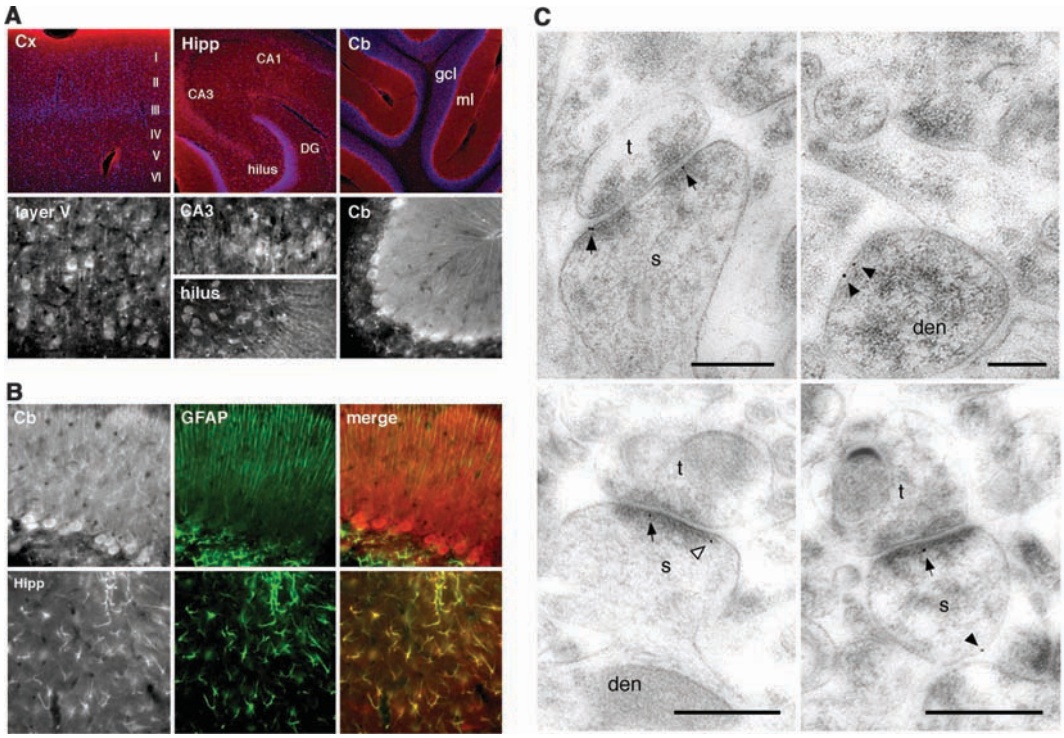

Fig. 3. Expression profile of CNIH-2 and CNIH-3 in CNS neurons and glial cells. (**A**) Immunostaining (red, top; white, bottom) of neocortex (Cx), hippocampal formation (Hipp) and cerebellum (Cb) with anti–CNIH-2/3. Immunoreactivity was observed in various cell types throughout the cortical layers (including both pyramidal and stellate cells in layer V), in CA1/CA3 pyramidal cells and subpopulations of hilar neurons in the hippocampus (including mossy cells), and in Purkinje neurons, as well as in the molecular layer (ml) of the cerebellum. Granule cells in the cerebellum (granule cell layer, gcl) were not stained. DG, dentate gyrus. DAPI staining of nuclei is in blue. (**B**) CNIH-2/3 immunoreactivity in radial Bergmann glia in the cerebellum (upper left) and hippocampal astrocytes (lower left) identified by double-labeling with an antibody against the glial fibrillary acidic protein (GFAP, middle, and both signals merged, right). (**C**) Electron micrographs of CNIH-2/3 immunoreactivity in the CA1 region of the adult rat hippocampus detected by post-embedding immunogold-EM. Immunoparticles were found over (arrows) and at the edge (open arrowhead) of asymmetrical synapses between axon terminals (t) and dendritic spines (s) of pyramidal cells. Gold particles were also found at the extrasynaptic plasma membrane (filled arrowheads) of dendritic shafts (den) and spines of pyramidal cells. Scale bars, 0.2 μm.

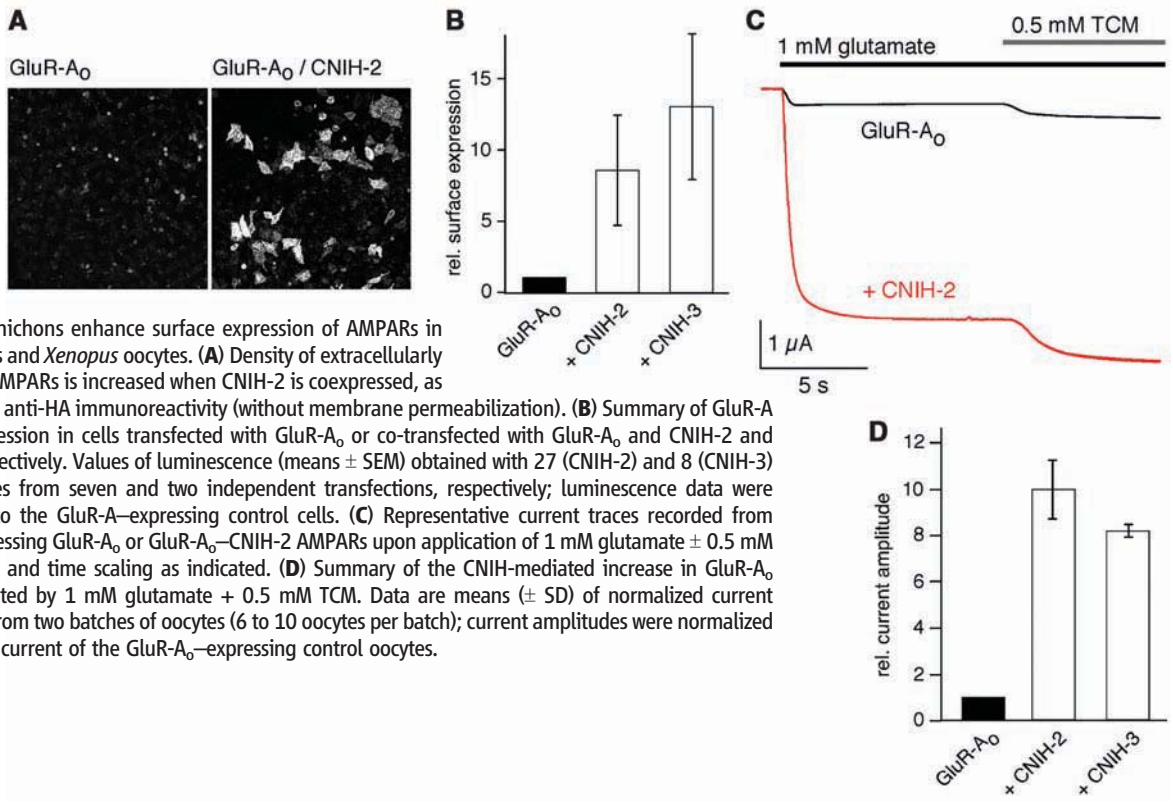

Fig. 4. Cornichons enhance surface expression of AMPARs in cultured cells and *Xenopus* oocytes. (**A**) Density of extracellularly HA-tagged AMPARs is increased when CNIH-2 is coexpressed, as visualized by anti-HA immunoreactivity (without membrane permeabilization). (**B**) Summary of GluR-A surface expression in cells transfected with GluR-A_o or co-transfected with GluR-A_o and CNIH-2 and CNIH-3, respectively. Values of luminescence (means ± SEM) obtained with 27 (CNIH-2) and 8 (CNIH-3) culture dishes from seven and two independent transfections, respectively; luminescence data were normalized to the GluR-A–expressing control cells. (**C**) Representative current traces recorded from oocytes expressing GluR-A_o or GluR-A_o–CNIH-2 AMPARs upon application of 1 mM glutamate ± 0.5 mM TCM; current and time scaling as indicated. (**D**) Summary of the CNIH-mediated increase in GluR-A_o currents elicited by 1 mM glutamate + 0.5 mM TCM. Data are means (± SD) of normalized current amplitudes from two batches of oocytes (6 to 10 oocytes per batch); current amplitudes were normalized to the mean current of the GluR-A_o–expressing control oocytes.

varied according to its expression level (Fig. 5A and fig. S5). Closer analysis (of the current decay) revealed that the slowing of deactivation by γ-2 and CNIH-2 resulted from a more complex process of channel closure. Although the deactivation time course of GluR-A_i/B_i receptors was adequately described by a single exponential function (time constant of 0.96 ± 0.24 ms, n = 15) (Fig. 5D), two exponential components were required for adequate fitting of the current decay in accessory subunit–containing GluR-A_i/B_i receptor complexes (Fig. 5, B and D) [see also (*36*)]. The distinct effects of γ-2 and CNIH-2 on deactivation kinetics predominantly resulted from the distinct amplitudes of the respective slow component, which was 8 ± 4% (n = 5) in γ-2–containing complexes, but 30 ± 7% (n = 13) in GluR-A_i/B_i–CNIH-2 receptors ($P < 0.01$, Mann-Whitney U test) (Fig. 5D). At lower expression levels of CNIH-2, this slow component was largely reduced, and deactivation could be approximated with a monoexponential function albeit with a time constant for deactivation ($\tau_{deactivation}$) slower than that of GluR-A_i/B_i (fig. S5). As CNIH-2 did, CNIH-3 also prolonged deactivation kinetics of heteromeric GluR-A_i/B_i receptors (Fig. 5D).

The impact of the cornichon proteins on channel gating was also examined in AMPARs assembled from the flop splice variants of GluR-B and GluR-D (GluR-B_o/D_o), heteromeric channels that display the fastest deactivation and desensitization kinetics of AMPARs (*19*). Both CNIH-2 and CNIH-3 slowed the deactivation kinetics ~3.6-fold (Fig.

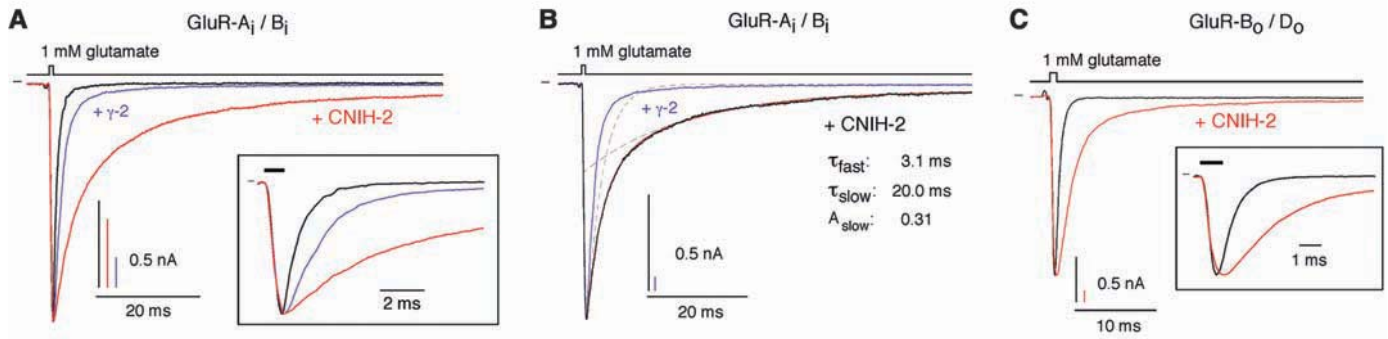

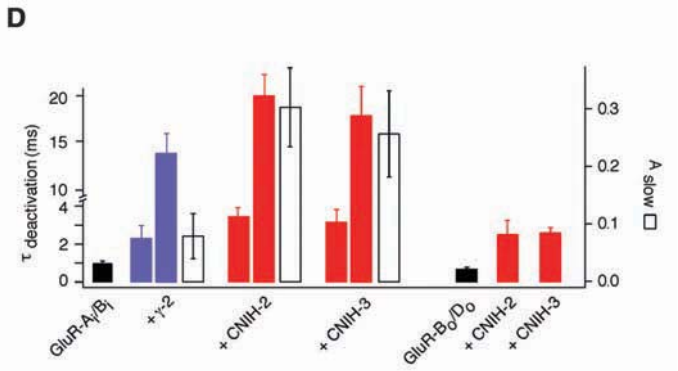

Fig. 5. Cornichons slow deactivation kinetics of AMPARs. (**A**) Representative current responses of AMPARs recorded upon 1-ms applications of 1 mM glutamate (indicated above the current trace) in giant oo-patches excised from *Xenopus* oocytes expressing GluR-A_i/B_i (black trace) or coexpressing GluR-A_i/B_i and either γ-2 (blue trace) or CNIH-2 (red trace). All complementary RNAs were injected at equal amounts; current and time scaling as indicated. (Inset) Current responses at expanded time scale; agonist application indicated by the horizontal bar. (**B**) Channel deactivation of GluR-A_i/B_i–CNIH-2 AMPAR complexes is a bi-exponential process. Continuous red line is fit of the sum of two exponentials (dashed lines, single components) with the time constants (τ_{fast}, τ_{slow}) and relative amplitude of the slow component (A_{slow}) as indicated. The current response of GluR-A_i/B_i–γ-2 complexes from (A) is shown for comparison. (**C**) Representative responses of GluR-B_o/D_o and GluR-B_o/D_o–CNIH-2 AMPARs upon 1-ms applications of 1 mM glutamate in experiments as in (A). (**D**) Summary of the fit parameters of channel deactivation obtained with AMPARs of the indicated molecular composition. Data are means (± SD) of 6 to 15 patches. Time constants are shown as solid bars, open bars denote A_{slow} in GluR-A_i/B_i–containing AMPARs.

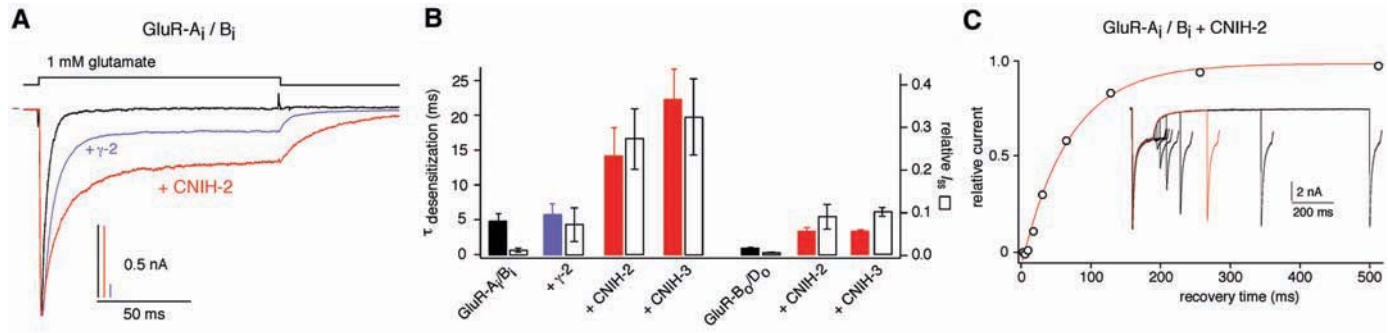

Fig. 6. Cornichons reduce desensitization of AMPARs without affecting recovery from desensitization. (**A**) Superimposed current responses of the indicated AMPARs to a 100-ms application of 1 mM glutamate (indicated above the current trace) in experiments as in Fig. 5. (**B**) Summary of the values for $\tau_{desensitization}$ (solid bars) and the relative amplitude of the nondesensitizing current component (relative I_{ss}, white bars) obtained from monoexponential fits to the current decay recorded from the indicated AMPARs in experiments as in (A). Data are means (± SD) of 6 to 15 patches. (**C**) Recovery of GluR-A_i/B_i–CNIH-2 AMPARs from steady-state desensitization recorded with a double-pulse protocol (pair of a 100-ms and a 50-ms glutamate pulse separated by increasing time intervals) in a giant oo-patch. Data points are peak currents recorded during the second pulse and normalized to the maximal current (recorded during the first glutamate application). Red line is the result of a monoexponential fit to the data points ($\tau_{recovery}$ = 69.2 ms). (Inset) Original current recordings; red trace is response with a recovery interval of 128 ms. (**D**) Values for $\tau_{recovery}$ obtained from fits as in (C) with the indicated AMPARs. Data are means (± SD) of three to eight patches.

5, C and D) ($\tau_{deactivation}$ of 0.71 ± 0.11 ms, $n = 8$ for pure GluR-B_o/D_o; 2.56 ± 0.74 ms, $n = 11$ and 2.61 ± 0.29 ms, $n = 7$ for GluR-B_o/D_o receptors coassembled with CNIH-2 and CNIH-3, respectively; $P < 0.001$ for CNIH-mediated effects, Mann-Whitney U test). As before, channel activation appeared largely unaffected by the CNIH proteins, as indicated by the similar values obtained for the 20 to 80% rise time in pure and CNIH-2–associated GluR-B_o/D_o receptors (values of 0.23 ± 0.02 ms, $n = 8$ for GluR-B_o/D_o; 0.28 ± 0.04 ms, $n = 11$ and 0.28 ± 0.05 ms, $n = 7$ for the receptors associated with CNIH-2 and CNIH-3, respectively). The differences in the time-to-peak interval observed between GluR-B_o/D_o receptors expressed alone and their CNIH-associated counterparts [(Fig. 5C), inset] likely reflected effects of the cornichons on both deactivation and desensitization, rather than differences in activation kinetics between both types of receptors (*45*).

In a second set of experiments, we therefore investigated the effects of CNIH-2 and CNIH-3 on the desensitization of GluR-A_i/B_i and GluR-B_o/D_o AMPARs, using 100-ms pulses of 1 mM glutamate. Representative current responses of such experiments (Fig. 6A) illustrate the changes caused by the coassembly of GluR-A_i/B_i receptors with CNIH-2. Thus, CNIH-2 markedly slowed the desensitization-mediated decay of the current and introduced a prominent nondesensitizing steady-state current component (Fig. 6A). When analyzed by monoexponential fits, the changes mediated by CNIH-2 and CNIH-3 in GluR-A_i/B_i receptors quantified to a more than threefold increase of the desensitization time constant ($\tau_{desensitization}$) and to a steady-state current of roughly 30% of the peak current (Fig. 6B); both the change in $\tau_{desensitization}$ and the amplitude of the nondesensitizing current depended on the expression level of CNIH-2 (fig. S5). A similar relative increase in $\tau_{desensitization}$ was obtained with the GluR-B_o/D_o receptors when assembled with the two cornichon isoforms (values for $\tau_{desensitization}$ of 0.92 ± 0.14 ms, $n = 8$ for GluR-B_o/D_o; 3.36 ± 0.51 ms, $n = 11$ and 3.48 ± 0.18 ms, $n = 6$ for GluR-B_o/D_o–CNIH-2 and GluR-B_o/D_o–CNIH-3, respectively; $P < 0.001$ for CNIH-mediated effects, Mann-Whitney U test); the respective steady-state current, however, was markedly smaller than in GluR-A_i/B_i receptors (~10% for both cornichon isoforms, Fig. 6B).

Because the CNIH proteins slowed desensitization, the reverse process, recovery from desensitization, was investigated with a double-pulse protocol in GluR-A_i/B_i and GluR-B_o/D_o receptors (*46*). As exemplified for GluR-A_i/B_i coassembled with CNIH-2, recovery from desensitization was complete, and the time course of recovery was adequately described by a single exponential (Fig. 6C). Unlike the gating transitions described above, recovery from desensitization was largely independent of associated CNIH proteins (Fig. 6D).

Taken together, the results on channel kinetics indicated that the CNIH proteins extensively modify the gating properties of AMPARs, probably by stabilizing the open state of the receptor channels; this stabilizing effect promotes slowing of deactivation and desensitization, without major effects on channel activation or recovery from desensitization. Moreover, the channel gating observed with heterologously expressed GluR-A_i/B_i–CNIH receptors closely resembles that of their native counterparts from hippocampal mossy cells and CA3 pyramidal cells (fig. S5) (*16*).

Discussion. We identified cornichon homologs 2 and 3 as intrinsic auxiliary subunits of the majority of AMPAR complexes in the mammalian brain. Physical association of CNIH-2 and CNIH-3 with the pore-forming GluR proteins promotes surface expression of AMPARs and extensively modulates their gating properties by slowing deactivation and desensitization kinetics.

CNIH proteins—novel auxiliary subunits of AMPARs. For comprehensive analysis of the molecular composition of native AMPARs, we used a proteomic approach that combines APs of appropriately solubilized protein complexes (controlled by BN-PAGE) (Figs. 1A and 2A) with nano-LC MS/MS analysis of total eluates. When applied to membrane preparations from total rat brain, this procedure isolated the expected set of known AMPAR subunits including the four GluR proteins, as well as six members of the TARP family (table S1). This unbiased approach also revealed two unexpected results. First, it identified the two cornichon proteins CNIH-2 and CNIH-3 as copurified partners of native AMPARs (Fig. 1 and table S1); neither of these proteins has previously been implicated in AMPAR physiology. Second, by relative quantification of MS-data and electrophoretic analyses (Fig. 2), the proteomic approach showed that the two CNIH proteins coassemble with the majority of AMPARs in the rat brain. We estimate that ~70% of AMPARs contain cornichons as accessory subunits, whereas ~30% coassemble with TARPs (Fig. 2). Antibody-shift assays (Fig. 2 and fig. S4) and APs with the anti–γ-2/3 and anti–CNIH-2/3 antibodies suggest that a minor portion of AMPARs may be coassembled with both TARPs and cornichons; in the majority of AMPARs, however, both accessory subunits seemed to be mutually exclusive.

Subsequent functional analysis showed that both cornichon proteins affect surface expression and gating properties of AMPARs in the plasma membrane (Figs. 4 to 6). These AMPAR-related functions are different from what has been reported for this family of proteins in *Drosophila*, chicken, and yeast, where cornichons were shown to operate as cargo receptors for the export of certain growth factors from the endoplasmic reticulum (*37*, *38*, *47*). Thus, it appears that the members of the cornichon family of transmembrane proteins may have multiple functions in cell physiology.

Implication for AMPAR-mediated signaling in the CNS. The influence of CNIH-2 and CNIH-3 on the gating of AMPARs may be viewed as stabilization of the open state impairing channel closure either upon agonist removal or upon conformational processes that trigger receptor desensitization (*48*). As a consequence, the time course of both deactivation and desensitization was slowed by up to several-fold in AMPARs of various subunit composition (Figs. 5 and 6).

Immuno-EM on the hippocampal CA1 region (Fig. 3C) suggests that CNIH proteins may be incorporated into both postsynaptic and extrasynaptic AMPARs. If coassembled into postsynaptic AMPARs, the cornichons will slow the decay time course of EPSCs, often determined by AMPAR deactivation kinetics. If present in extrasynaptic receptors, CNIH-2 and 3 may enhance the effects of glutamate spillover from the release sites to more distant locations, leading to the activation of receptors that would otherwise desensitize. Such spillover effects may be relevant in mossy fiber synapses on hippocampal CA3 pyramidal neurons and hilar mossy cells and in parallel and climbing fiber synapses on cerebellar Purkinje cells, in which the presynaptic elements form closely spaced release sites (*49*, *50*) and the postsynaptic neurons abundantly express the two cornichon proteins (Fig. 3). Thus, effects on postsynaptic and extrasynaptic receptors will slow EPSCs, prolonging the time course of excitatory postsynaptic potentials and thus enhancing temporal summation of synaptic events (fig. S6). Whether neurons specialized on synaptic integration (such as hippocampal pyramidal cells) and others specialized on coincidence detection (such as neurons in the auditory pathway or GABAergic interneurons in the cortex) differentially express the cornichon proteins remains to be determined. In conclusion, our results establish cornichons CNIH-2 and CNIH-3 as a new class of accessory AMPAR subunits and thus provide novel molecular determinants for the modulation of neurotransmission in the CNS.

References and Notes

1. P. Jonas, N. Spruston, *Curr. Opin. Neurobiol.* **4**, 366 (1994).
2. I. M. Raman, L. O. Trussell, *Neuron* **9**, 173 (1992).
3. P. Sah, S. Hestrin, R. A. Nicoll, *J. Physiol.* **430**, 605 (1990).
4. R. A. Silver, S. F. Traynelis, S. G. Cull-Candy, *Nature* **355**, 163 (1992).
5. M. Sheng, M. J. Kim, *Science* **298**, 776 (2002).
6. I. Song, R. L. Huganir, *Trends Neurosci.* **25**, 578 (2002).
7. F. Conti, R. J. Weinberg, *Trends Neurosci.* **22**, 451 (1999).
8. P. Jonas, *News Physiol. Sci.* **15**, 83 (2000).
9. J. Boulter *et al.*, *Science* **249**, 1033 (1990).
10. K. Keinänen *et al.*, *Science* **249**, 556 (1990).
11. S. Nakanishi, *Science* **258**, 597 (1992).
12. G. L. Collingridge, R. W. Olsen, J. Peters, M. Spedding, *Neuropharmacology* **56**, 2 (2009).
13. R. Dingledine, K. Borges, D. Bowie, S. F. Traynelis, *Pharmacol. Rev.* **51**, 7 (1999).
14. P. H. Seeburg, M. Higuchi, R. Sprengel, *Brain Res. Brain Res. Rev.* **26**, 217 (1998).
15. B. Sommer *et al.*, *Science* **249**, 1580 (1990).
16. J. R. P. Geiger *et al.*, *Neuron* **15**, 193 (1995).
17. M. Hollmann, M. Hartley, S. Heinemann, *Science* **252**, 851 (1991).
18. H. Lomeli *et al.*, *Science* **266**, 1709 (1994).
19. J. Mosbacher *et al.*, *Science* **266**, 1059 (1994).
20. A. S. Kato, E. R. Siuda, E. S. Nisenbaum, D. S. Bredt, *Neuron* **59**, 986 (2008).
21. A. D. Milstein, W. Zhou, S. Karmizadegan, D. S. Bredt, R. A. Nicoll, *Neuron* **55**, 905 (2007).

22. C. H. Cho, F. St-Gelais, W. Zhang, S. Tomita, J. R. Howe, *Neuron* **55**, 890 (2007).
23. D. Soto, I. D. Coombs, L. Kelly, M. Farrant, S. G. Cull-Candy, *Nat. Neurosci.* **10**, 1260 (2007).
24. S. Tomita *et al*., *Nature* **435**, 1052 (2005).
25. W. Vandenberghe, R. A. Nicoll, D. S. Bredt, *Proc. Natl. Acad. Sci. U.S.A.* **102**, 485 (2005).
26. C. Bats, L. Groc, D. Choquet, *Neuron* **53**, 719 (2007).
27. L. Chen *et al*., *Nature* **408**, 936 (2000).
28. K. Menuz, G. A. Kerchner, J. L. O'Brien, R. A. Nicoll, *Neuropharmacology* **56**, 22 (2009).
29. K. Menuz, J. L. O'Brien, S. Karmizadegan, D. S. Bredt, R. A. Nicoll, *J. Neurosci.* **28**, 8740 (2008).
30. M. Fukaya, M. Yamazaki, K. Sakimura, M. Watanabe, *Neurosci. Res.* **53**, 376 (2005).
31. N. Klugbauer *et al*., *FEBS Lett.* **470**, 189 (2000).
32. H. Berkefeld *et al*., *Science* **314**, 615 (2006).
33. J. Liu, J. Xia, K. H. Cho, D. E. Clapham, D. Ren, *J. Biol. Chem.* **282**, 18945 (2007).
34. M. S. Nadal *et al*., *Neuron* **37**, 449 (2003).
35. U. Schulte *et al*., *Neuron* **49**, 697 (2006).
36. Materials and methods are available as supporting material on *Science* Online.
37. C. Bokel, S. Dass, M. Wilsch-Brauninger, S. Roth, *Development* **133**, 459 (2006).
38. H. Hoshino *et al*., *Mol. Biol. Cell* **18**, 1143 (2007).
39. S. Roth, F. S. Neuman-Silberberg, G. Barcelo, T. Schupbach, *Cell* **81**, 967 (1995).
40. L. Chen, S. Bao, X. Qiao, R. F. Thompson, *Proc. Natl. Acad. Sci. U.S.A.* **96**, 12132 (1999).
41. K. Hashimoto *et al*., *J. Neurosci.* **19**, 6027 (1999).
42. B. Hille, *Ion Channels of Excitable Membranes* (Sinauer Associates, Sunderland, MA, ed. 3, 2001).
43. D. Turetsky, E. Garringer, D. K. Patneau, *J. Neurosci.* **25**, 7438 (2005).
44. C. Antz *et al*., *Nat. Struct. Biol.* **6**, 146 (1999).
45. D. S. Koh, J. R. Geiger, P. Jonas, B. Sakmann, *J. Physiol.* **485**, 383 (1995).
46. D. Colquhoun, P. Jonas, B. Sakmann, *J. Physiol.* **458**, 261 (1992).
47. C. P. Castro, D. Piscopo, T. Nakagawa, R. Derynck, *J. Cell Sci.* **120**, 2454 (2007).
48. Y. Sun *et al*., *Nature* **417**, 245 (2002).
49. B. Barbour, M. Häusser, *Trends Neurosci.* **20**, 377 (1997).
50. A. Rollenhagen *et al*., *J. Neurosci.* **27**, 10434 (2007).
51. We thank J. P. Adelman for insightful comments and critical reading of the manuscript and A. Haupt for help with bioinformatics. This work was supported by grants of the Deutsche Forschungsgemeinschaft to B.F. (SFB 746/TP16, SFB780/TPA3, EXC 294) and to N.K. (SFB780/TPB4).

Supporting Online Material

www.sciencemag.org/cgi/content/full/323/5919/1313/DC1
Materials and Methods
Figs. S1 to S6
Table S1
References

29 October 2008; accepted 16 January 2009
10.1126/science.1167852

Brightly Fluorescent Single-Walled Carbon Nanotubes via an Oxygen-Excluding Surfactant Organization

Sang-Yong Ju,[1] William P. Kopcha,[2] Fotios Papadimitrakopoulos[1,2]*

Attaining high photoluminescence quantum yields for single-walled carbon nanotubes (SWNTs) in order to broaden their optoelectronics and sensing applications has been a challenging task. Among various nonradiative pathways, sidewall chemisorption of oxygen provides a known defect for exciton quenching through nanotube hole doping. We found that an aliphatic (dodecyl) analog of flavin mononucleotide, FC12, leads to high dispersion of SWNTs, which tend to aggregate into bundles. Unlike other surfactants, the surface organization of FC12 is sufficiently tight to exclude oxygen from the SWNT surface, which led to quantum yields as high as 20%. Toluene-dispersed, FC12-wrapped nanotubes exhibited an absorption spectrum with ultrasharp peaks (widths of 12 to 25 milli–electron volts) devoid of the characteristic background absorption of most nanotube dispersions.

The ability to readily assign the (*n*,*m*) chirality of semiconducting single-walled carbon nanotubes (SWNTs) by means of photoluminescence excitation (PLE) mapping (*1*), together with their photostability (*2*), holds promise for applications in optoelectronics (*3*), biological imaging (*2*, *4*), and sensing (*4*). Although the optical properties of SWNTs are excitonic in nature (*5*), these structures exhibit low-fluorescence quantum yields. Possible causes include low-lying, nonradiative states (dark excitons) (*6*) or various defects that, as a result of the large exciton diffusion length (~90 nm) in SWNTs, contribute to substantial photoluminescence quenching (*7*, *8*). Oxygen in particular, in the presence of an acid or neutral environment (*9*), can quench photoluminescence through hole doping and subsequent nonradiative Auger recombination (*8*, *10*).

To make matters worse, nanotube bundling (*11*, *12*), along with chemical defects resulting from covalent functionalization (*13*) and nanotube inhomogeneities (*14*), can further decrease or completely quench nanotube luminescence. Individual SWNTs can have photoluminescence quantum yields as high as 8% (*15*), but solution-suspended SWNTs have shown much lower quantum yields [i.e., 1.5% for polyfluorene (PFO)–wrapped SWNTs (*16*), 1.1% for purified DNA-wrapped SWNTs (*11*), and less than 0.1% for surfactant-micellarized nanotubes (*16*, *17*)]. Most SWNT surfactants allow oxygen to interact and dope these nanotubes, and are sufficiently labile that they allow the nanotubes to reform bundles (*9*). Here, we show that a low-molecular-weight, organic-soluble analog of flavin mononucleotide, FC12, imparts considerable individualization in toluene and other aromatic solvents (i.e., *o*-xylene and benzene). In addition, the tight self-organization of FC12 around SWNTs leads to an effective exclusion of oxygen that affords quantum yields as high as 20%.

Flavin mononucleotide (FMN), a common redox cofactor related to vitamin B_2, was recently shown to self-organize around SWNTs through a helical conformation (*18*). Such helical wrapping (Fig. 1, A and B) originates from two sets of self-recognizing H-bonds that "stitch" the neighboring FMN moieties into a continuous helical ribbon (Fig. 1A), the concentric π-π interaction of the isoalloxazine ring with the underlying graphene sidewalls (Fig. 1B), and a soluble *d*-ribityl phosphate side group that imparts effective solubilization in aqueous media. In an effort to broaden flavin-based dispersion in organic solvents, we synthesized an isoalloxazine derivative with an aliphatic (dodecyl) side group, termed FC12. The synthetic route of FC12 involves two facile steps with an overall yield of ~35% (*19*). FC12 dispersions of CoMoCAT (Co-Mo bimetallic catalyst synthesized) SWNTs (*20*) were obtained by sonicating 1 mg of FC12, 1 mg of SWNTs, and 4 ml of various solvents for 4 hours at 300 W. The mixture was centrifuged for 20 min at 10,000*g*, which eliminated visible SWNT bundles in various solvents [i.e., benzene, toluene, *o*-xylene, ethylacetate, tetrahydrofuran (THF), pyridine, acetone, and *N*,*N*-dimethyl formamide (DMF)]. Table 1 summarizes the physical properties of these solvents as a function of dielectric constant (ε). SWNT photoluminescence was observed for only some of these solvents: benzene, toluene, *o*-xylene, ethylacetate, THF, and acetone (see below).

PLE maps for benzene, toluene, ethylacetate, and acetone show that the photoluminescence intensity (~315,000 counts) of FC12–(6,5)-SWNTs in toluene dispersion is 15 to 20 times

[1]Nanomaterials Optoelectronics Laboratory, Polymer Program, University of Connecticut, Storrs, CT 06269, USA. [2]Department of Chemistry, Institute of Materials Science, University of Connecticut, Storrs, CT 06269, USA.

*To whom correspondence should be addressed. E-mail: papadim@mail.ims.uconn.edu